Chronic arthritis directly induces quantitative and qualitative bone disturbances leading to compromised biomechanical properties

J. Caetano-Lopes[1], A.M.Nery[1,2,3], R. Henriques[4,5], H. Canhão[1,6], J. Duarte[7,8], P.M. Amaral[2,3], M. Vale[1,9], R.A. Moura[1], P.A. Pereira[1], P. Weinmann[1], S. Abdulghani[1], M. Souto-Carneiro[8], P. Rego[9], J. Monteiro[9], S. Sakagushi[10], M.V. Queiroz[6], Y.T. Konttinen[11], L. Graça[7,8], M.F. Vaz[2,3], J.E. Fonseca[1,6]

[1]Rheumatology Research Unit, Instituto de Medicina Molecular, Faculdade de Medicina da Universidade de Lisboa, Lisbon, Portugal; [2]Instituto de Ciência e Engenharia de Materiais e Superfícies, Instituto Superior Técnico, Lisbon, Portugal; [3]Departamento de Engenharia de Materiais, Instituto Superior Técnico, Lisbon, Portugal; [4]Unidade de Biologia Celular, Instituto de Medicina Molecular, Faculdade de Medicina da Universidade de Lisboa, Lisbon, Portugal; [5]Instituto de Sistemas e Robótica, Instituto Superior Técnico, Lisbon, Portugal; [6]Serviço de Reumatologia e Doenças Ósseas Metabólicas, Hospital de Santa Maria, Lisbon, Portugal; [7]Cellular Immunology Unit, Instituto de Medicina Molecular, Faculdade de Medicina, Universidade de Lisboa, Lisbon, Portugal; [8]Instituto Gulbenkian de Ciência, Oeiras, Portugal; [9]Serviço de Ortopedia, Hospital de Santa Maria, Lisbon, Portugal; [10]Department of Experimental Pathology, Institute for Frontier Medical Sciences, Kyoto University, Kyoto 606-8507, Japan; [11]University of Helsinki, ORTON Orthopaedic Hospital of the Invalid Foundation, Helsinki, COXA Hospital for Joint Replacement, Tampere, Finland.

Abstract

Objectives

Rheumatoid arthritis (RA) is associated with an increased risk of fragility fractures. In RA patients, the direct effect of inflammation on bone is difficult to study because their skeleton is also affected by medication with corticosteroids and other drugs as well as aging and menopause, which contribute to bone fragility. This study used an animal model of chronic arthritis to evaluate the direct impact of chronic inflammation on biomechanical properties and structure of bone.

Methods

In the SKG mouse chronic arthritis model three point bending tests were performed on femoral bones and compression tests on vertebral bodies. Collagen structure was analysed using second-harmonic generation (SHG) imaging with a two-photon microscope, ultramorphology by scanning electron microscopy (SEM) coupled with energy dispersive x-ray spectroscopy (EDS) and bone density using water pycnometer.

Results

Arthritic bones had poor biomechanical quality compared to control bones. SHG, SEM and pycnometry disclosed variable signs of impaired collagen organization, poor trabecular architecture and low bone density.

Conclusion

Present data demonstrate for the first time that chronic inflammation per se, without confounding influence of drugs and aging, leads to impairment of bone biomechanics in terms of stiffness, ductility and ultimate strength (fracture).

Key words

Rheumatoid arthritis, SKG mice, osteoporosis, bone, mechanical tests, multiphoton microscopy.

*Joana Caetano-Lopes, PhD student**
*Ana Margarida Nery, MSc**
Ricardo Henriques, PhD student
Helena Canhão, MD, PhD
Joana Duarte, PhD student
Pedro M. Amaral, PhD
Mário Vale, MD
Rita A. Moura, PhD student
Patrícia A. Pereira, MSc
Pamela Weinmann, PhD
Saba Abdulghani, PhD
Margarida Souto-Carneiro, PhD
Paulo Rego, PhD
Jacinto Monteiro, MD, PhD
Shimon Sakagushi, PhD
Mário Viana Queiroz, MD, PhD
Yrjö T. Konttinen, MD, PhD
Luís Graça, MD, PhD
Maria Fátima Vaz, PhD
João Eurico Fonseca, MD, PhD

**Both authors contributed equally to this study.*

This work was supported by the PTDC/SAU-BEB/65992/2006 grant from Fundação para a Ciência e Tecnologia.

Please address correspondence and reprint requests to:
João Eurico Fonseca,
Rheumatology Research Unit,
Instituto de Medicina Molecular,
Edifício Egas Moniz,
Faculdade de Medicina da Universidade de Lisboa, Av. Professor Egas Moniz, 1649-028 Lisboa, Portugal.
E-mail: jefonseca@netcabo.pt

Received on November 19, 2008; accepted in revised form on March 3, 2009.

© Copyright CLINICAL AND EXPERIMENTAL RHEUMATOLOGY 2009.

Conflict of interest: Dr Y.T. Konttinen has received support from the Sigrid Jusélius Foundation, evo grants, Finska Läkaresällskapet and the ORTON Foundation; the other co-authors have declared no competing interests.

Introduction

Rheumatoid arthritis (RA) is a chronic inflammatory disease, of unknown aetiology, which affects around 1% of the world-population (1). Bone erosions can develop in the first few months of the disease. These bone erosions are caused by the inflammatory synovial membrane, which attaches to the joint surface (*pannus*) and invade cartilage and bone (2). Recent evidences suggest that bone remodelling disturbances also contribute to bone erosions and in particular to the development of secondary osteoporosis (OP). In fact, RA patients have an increased risk of vertebral fractures, which is independent from bone mineral density and corticosteroid use (3). In addition, an elevated hip fracture risk was also noted in RA patients not exposed to corticosteroids (4). Thus, RA seems in itself to predispose to fractures although the underlying mechanisms and their effects on bone are not completely understood yet.

The connection between OP and RA can be partially explained by the activation of the Receptor Activator of Nuclear Factor κB (RANK) by RANK Ligand (RANKL) (5) produced by activated T lymphocytes (6) and osteoblasts (7). This activates signalling leading to pre-osteoclast priming and osteoclast activation, which contribute to the formation of bone erosions and reduction of the bone mineral density. RANK/RANKL interaction is antagonised by osteoprotegerin (OPG) (5), a soluble decoy receptor. In RA the RANKL/OPG ratio is increased (8).

Osteoclasts dissolve mineralized bone matrix (mainly hydroxyapatite crystals) and destroy the exposed non-mineralized organic bone matrix (mainly type I collagen) (9). However, it is not clear if, how, and to what extent the bone structure itself is affected by inflammation although it is known that the arrangement of bone trabeculae and the orientation of collagen fibres and hydroxyapatite crystals in relation to load play an important role for bone strength (10). The main objective of the present work was to study to what extent the biomechanical properties of bone are influenced by the destructive arthritic changes.

Due to multiple confounding factors involved, like the use of glucocorticosteroids and other drugs as well as aging and hormonal changes, it is difficult to specifically study the effect of arthritis *per se* on the structure and biomechanics of bone in RA. The use of a mouse model of chronic arthritis would reduce such variability and allow access to bones for *ex vivo* testing. Animal models are already widely used in the development of new drugs for OP (11). The recently described SKG mouse arthritis model resembles in many aspects human RA. These mice develop a rheumatoid factor positive, erosive chronic polyarthritis that affects both large and small joints and present some of the systemic features of RA. The SKG mouse has a BALB/c background (12) with a single recessive point mutation in the ZAP-70 gene, a G→T substitution that alters codon 163 from tryptophan to cystein. This gene encodes a protein, which has an important role for T cell signal transduction and its mutation leads to changes in the thymic selection threshold. As a result SKG mice maintain otherwise negatively selected autoreactive T cell clones. Unlike their normal BALB/c counterparts, SKG mice are genetically prone to spontaneously develop chronic polyarthritis, the onset of which can be precipitated by zymosan or by other dectin-1 agonist (12, 13). This experimental arthritis model was used to study the direct effect of chronic arthritis on bone structure and biomechanics.

Material and methods

SKG arthritis model and BALB/c controls

Twenty-five female SKG and sixteen female BALB/c mice were bred and maintained under pathogen free conditions. All experiments were conducted according to the guidelines from the Animal User and Institutional Ethics Committee. A single intraperitoneal injection of 2mg of zymosan (Sigma-Aldrich Co, USA) was administered at 2 months of age. Joint swelling was monitored by inspection as follows: 0, no joint swelling; 0.1, swelling of one finger joint; 0.5, mild swelling of wrist or ankle; and 1.0, severe swelling of

wrist or ankle, with a range of the total sum score varying from 0 to 5 (12). At five months the SKG and BALB/c mice were sacrificed and femoral bones and vertebrae were dissected free of soft tissues and stored at -20°C. Immediately before testing, the samples were defrosted at room temperature.

Mechanical testing

All mechanical tests were performed using a universal testing machine (Instron 5566™, Instron Corporation, Canton, USA) with a load cell of 500 N. The biomechanical strength variables were displayed in stress-strain curves by the Bluehill 2 Software (Instron, Copyright 1997-2007) and analysed using MatLab 7.1 software (R14 SP3, The Mathworks, Inc, Copyright 1984-2006). The software has the ability to build stress-strain representations from load-displacement points, once initial dimensions are provided for each specimen.

Femoral bones were submitted to three-point bending tests (Fig. 1A) and vertebrae to compression tests (Fig. 1B).

For three-point bending tests the span between the outer loading points was 5 mm with the load being applied to the centre of the femoral shaft at a cross-head speed of 0.01 mm/s. The parameters analysed from the stress-strain curves were Young's modulus (E), yield stress (σ_y), ultimate stress (σ_u), ultimate strain (ε_u) and work/energy until ultimate stress (W_u) (Fig. 1C).

The second (L2) and fourth (L4) lumbar vertebrae were used for compression tests. In these tests a cross head speed of 0.01 mm/s was used, and then obtained Young's modulus (E), yield stress (σ_y), maximum stress (σ_M), work until yield stress (W_y) and work until maximum stress (W_M) (Fig. 1D).

Assuming that femurs behave like cylinders (14), stress-strain curves can be built according to the following equations (1 and 2):

$$\sigma = \frac{L \cdot s}{\pi\left(d_f/2\right)^3} \quad (Pa) \qquad (1)$$

$$\varepsilon = \frac{12\left(d_f/2\right)\Delta l}{s^2} \cdot 100 \quad (\%) \qquad (2)$$

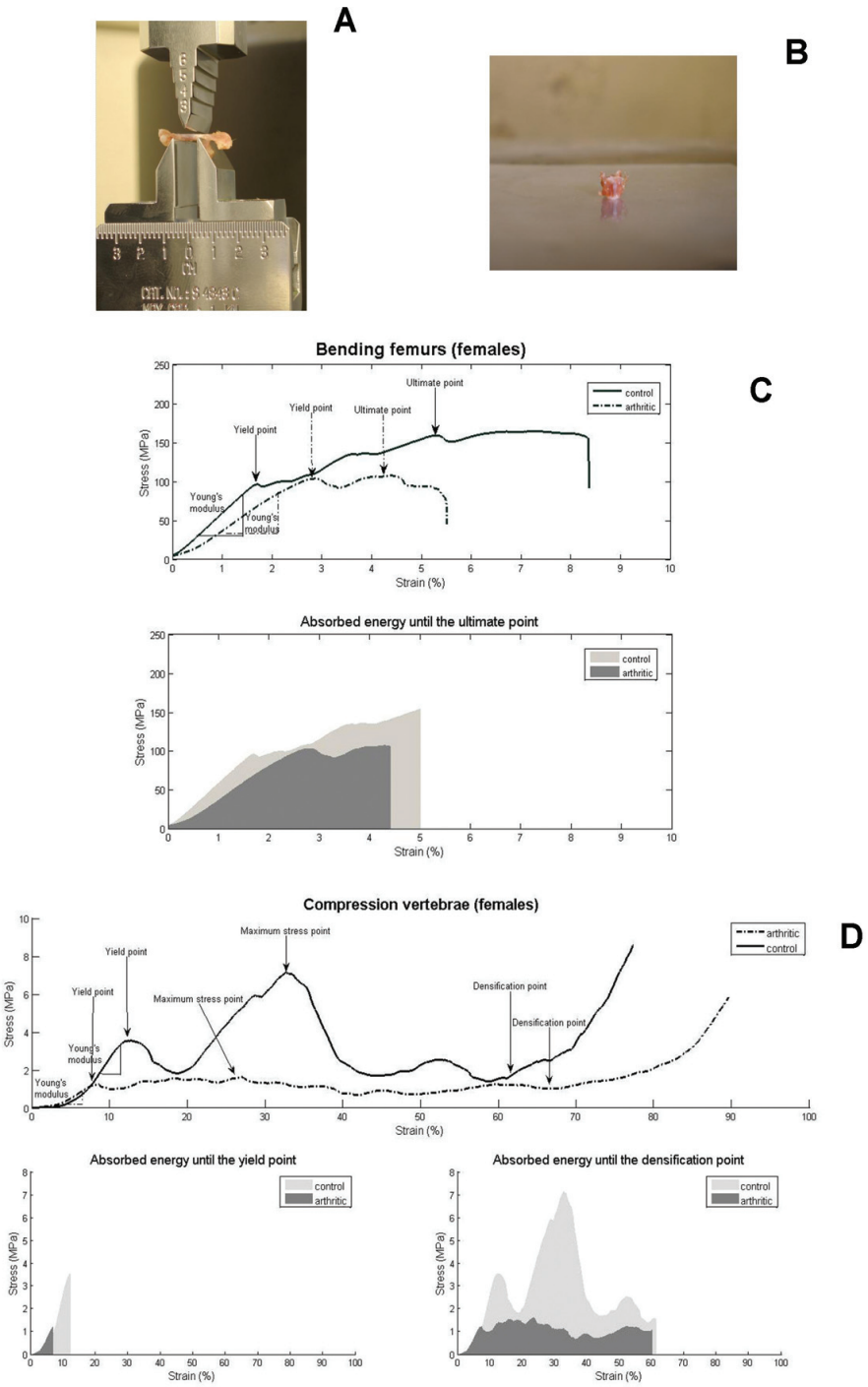

Fig. 1. Experimental setup and stress-strain representations obtained after mice femurs bending and vertebrae compression. Images of a three point bending test setup (**A**), and a vertebra standing on the inferior plate of a compression test setup (**B**). Femurs (arthritic and control) bending curves (**C**) were obtained in order to determine the analysed parameters directly from the graphic: Yield point=(yield strain, yield stress) and Ultimate point=(ultimate strain, ultimate stress), or after calculations:
Young's modulus – slope of the curve between the origin and the yield point;
Energy until ultimate point – area under the graphic from the origin until the ultimate point, calculated using trapezoidal numerical integration.
Vertebrae (arthritic and control) compression curves (**D**) were obtained from the mechanical test in order to determine the analysed parameters directly from the graphic: First yield point=(first yield strain, first yield stress), Second yield point = (second yield strain, second yield stress) and Densification point = (densification strain, densification stress), or after calculations:
Young's modulus – slope of the curve between the origin and the first yield point;
Energy until first yield, or densification points – area under the graphic from the origin until the first yield point or until densification point, calculated using trapezoidal numerical integration.

Where σ - stress (Pa); L = load (N); s = support span (mm); d_f = femoral outer diameter (mm); ε = strain (%); Δl = displacement (mm).

All the calculations were done for the middle cross-section area, applied to the centre of the femoral shaft, by the upper load support. From these curves the mechanical parameters were read, except for the Young's modulus, which was obtained from the slope of the elastic regime of the stress-strain curves, and the energies absorbed until determined points that were calculated using trapezoidal numerical integration, with using MatLab 7.1 software.

For vertebrae, compression tests were made (14). Equations (3 and 4) show how stress-strain curves can be obtained, assuming that a cylinder, of homogenous material, is being compressed:

$$\sigma = \frac{L}{\pi\left(d_v/2\right)^2} \quad (Pa) \tag{3}$$

$$\varepsilon = \frac{\Delta h}{h_0} \cdot 100 \quad (\%) \tag{4}$$

Where d_v = vertebral diameter (mm); h_0 = initial vertebral height (mm); Δh = compression suffered by the vertebra (displacement) (mm).

As for femurs, the biomechanical parameters were read from the stress strain curves and the Young's modulus as well as the energies calculated using MatLab 7.1 software.

Even though, in this paper, all the vertebrae tested refer to the same lumbar position (L2 and L4) and the long bones were all femurs, there was always variability in dimensions associated with the fact that each bone comes from a different animal. In order to normalize this parameter, and allow all samples to be compared against each other, instead of load (L) – displacement (d) values, we used stress (σ) – strain (ε) representations. Stress is the load applied on a sample, per area unit (a) (equations 1 and 3), and the strain is the deformation suffered, when compared with the initial dimension of the bone (equations 2 and 4).

In this study it was assumed that both femurs and vertebrae were similar to cylinders, but with different orientations and dimensions, according to the mechanical test (three point bending for femurs and compression for vertebrae) performed in each case.

In this way, the results from the control and arthritic groups could be compared between each other, even if the dimensions were different, because this effect was already contemplated in the stress-strain analysis.

Second-harmonic generation and two-photon excitation microscopy

Mice vertebrae and femurs were decalcified, embedded in paraffin, cut to 7μm sections using a microtome and deparaffinised to be inspected in a Zeiss LSM510 META laser scanning microscope featuring a Coherent Mira 900 femtosecond multiphoton excitation laser. Multicolour nonlinear microscopy of collagen was done through second-harmonic generation (SHG) using two-photon excitation (TPE). The signal was acquired by two opposing detectors: 1) the META spectral detector configured for bandpass detection between 390-430 nm collecting light from a Zeiss Fluar 20x/0.75 objective; this signal was associated with a green look up table (LUT) and is referred to as backward-SHG and 2) the non-descanned detector (NDD) collecting light from a Zeiss 0.8 numerical aperture (NA) condenser and filtered by a 390-430 nm bandpass filter; this signal was associated with the blue LUT and is referred to as forward-SHG. The backward-SHG channel detects the backscattered SHG signal and the forward-SHG channel the SHG receives the photons that are transmitted through the sample (15). The wavelength of the laser was set to 820 nm. The Jefferies' method (16) was applied to all acquired images to quantify the amount of trabecular area occupied by collagen detected by the forward-SHG channel (essentially mature polymerized collagen) and by collagen detected by the backward-SHG channel (mainly immature collagen fibril segments, indicating ongoing fibrillogenesis) (17).

Image analysis was done using NIH ImageJ software (W. Rasband, National Institute of Health, Bethesda, USA) by applying a 40-255cps intensity threshold for each channel to cover only the extracellular collagen matrix. All the trabecular area was covered using a lower 20-255cps threshold.

Scanning electron microscopy

Bone samples were inserted into an epoxidic and transparent resin and mounted in a mixture of Résine Mecaprex MA2 (04008) and Durisseur pour résine Mecaprex MA2 (Presi SA. Tavernolles, 38320 Brie & Angonnes, France) in 100:12 ratio. After 24 hours the surfaces of the vertebrae samples were polished using grid papers with 1000, 800, 600, 320 and 200 μm granulometries. After deposition of a uniform and thin gold layer the samples were observed with an electron beam energy of 25 keV in a scanning electron microscope (Hitachi model S2400 SEM. Hitachi, Ltd. Tokyo, Japan).

The images obtained were analysed with the software ImageJ, already mentioned for the MPM images. In this case the region of interest was the vertebral body, where pictures were taken and parameters such as the area occupied by trabeculae (%), inter-trabecular distance (μm), trabecular thickness ($\bar{t}$, μm) and cortical thickness ($\bar{c}$, μm) were determined. These measurements were made according to Heyn's and Jefferies' methods (16).

Energy dispersive x-ray spectroscopy

The energy dispersive x-ray spectroscopy (EDS) analysis was performed to measure the proportion of calcium and phosphorus in the bone samples using an analytical SEM with Rontec standard EDS detector (Hitachi S2400, Tokyo, Japan).

Density measurements

The densities of both femoral bones and vertebrae were measured prior to mechanical testing with a water pycnometer. The pycnometer was filled with water, with corrections being made to the ambient temperature following the Archimedes' principle. Bone density was calculated using equation (5):

$$\rho = (m_1 - m_0)\rho_L \frac{1}{(m_3 - m_0) - (m_2 - m_1)} \tag{5}$$

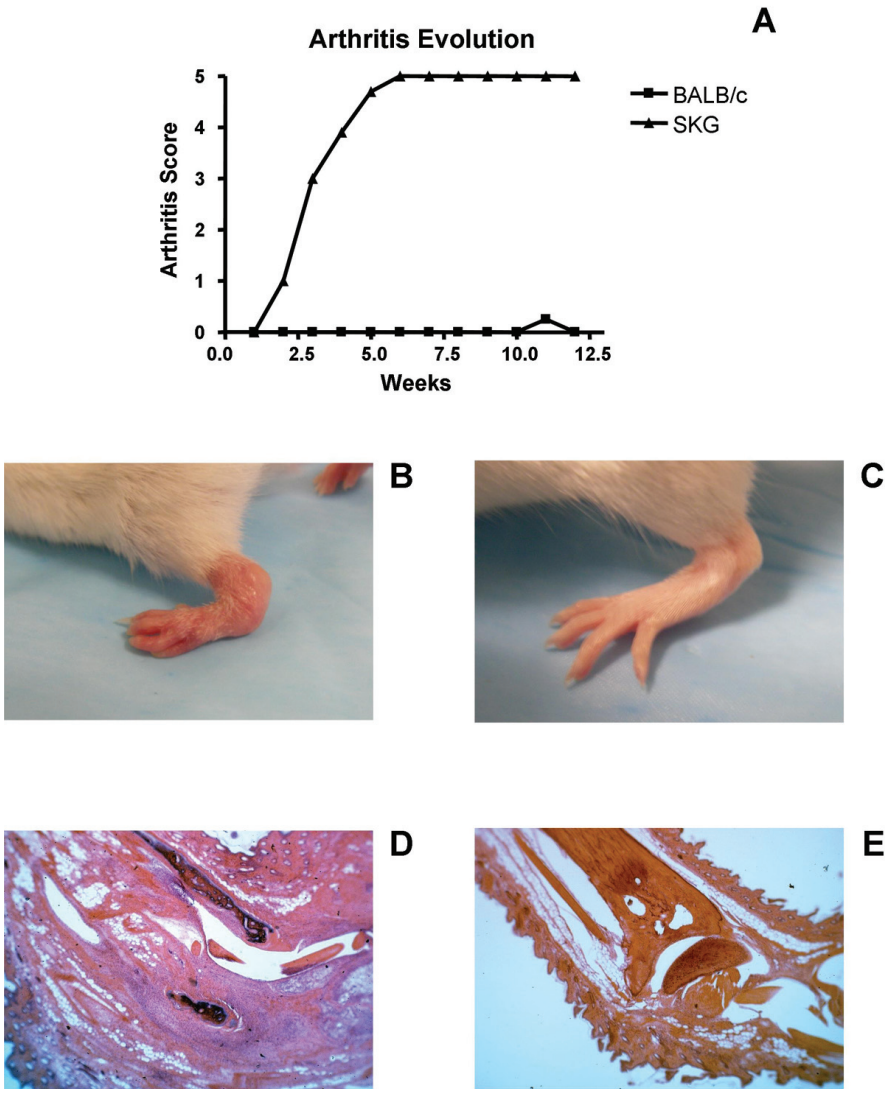

Fig. 2. SKG mice developed a severe destructive polyarthritis after zymosan injection. Joint swelling was monitored by inspection and scored as follows: 0: no joint swelling; 0.1: swelling of one finger joint; 0.5: mild swelling of wrist or ankle; and 1.0: severe swelling of wrist or ankle. Scores for all fingers and toes, wrists and ankles were totalled for each mouse. Graph (A) shows that the scores evaluation started at week zero and peak in the arthritis group at week 6 (squares and triangles represent median scores). BALB/c mice did not develop arthritis (**C**, **E**) and were used as controls to SKG mice (**B, D**), which showed evident swelling of the ankle joints and an erosive synovitis at 5 months of age (haematoxylin and eosin staining, magnification ×400).

Where ρ - bone density; ρ_L - water density at ambient temperature; m_0 - mass of the empty pycnometer; m_1 - mass of the pycnometer and the bone sample; m_2 - mass of the pycnometer, the bone sample and water; m_3 - mass of the pycnometer filled with water.

Statistical analysis

Results were represented by mean and standard deviation values. According to their distribution either t test for independent-samples or non–parametric Mann-Whitney test were used to compare continuous variables. Significance level was set at 0.05. Statistical analyses were performed using the Statistical Package for Social Sciences (SPSS) Manager software (SPSS, Inc, Chicago, IL, USA).

Results

Female SKG mice develop chronic arthritis

Twenty-five female SKG mice, injected with a single intraperitoneal injection of 2mg of zymosan at two months of age, developed chronic arthritis (in small and large joints) after one week and reached peak activity by the sixth week. By the time of sacrifice (5 months of age), the SKG mice had approximately 3 months of disease activity and all had a clinical score of 5. Inflammatory joint infiltration was severe and destructive (Fig. 2). The sixteen control BALB/c mice, after the 2mg zymosan injection, did not develop arthritis. These two strains of mice are identical, differing only in a point mutation in the ZAP-70 protein that only affects the selection of T lymphocytes in the thymus. BALB/c mice are widely used as a control for SKG mice.

A significant reduction in body weight of the SKG mice was observed in comparison to the BALB/c mice (18.60±1.04g and 24.08±0.81g respectively, $p<0.001$).

Chronic arthritis reduces mechanical properties of femurs and vertebrae

Mechanical 3-point bending test results (Table I and Fig. 1C) showed that arthritic femurs have a significantly lower: elastic (Young's) modulus (reflecting reduced stiffness), yield stress (less force was needed to cause the first microfractures and to start a plastic and definitive deformation of bone), ultimate stress (reflecting the maximum strength of the bone at fracture) and energy until ultimate stress (reflecting the energy required to cause fracture, thus the toughness of the bone) as compared to control femurs.

In the case of vertebrae compression tests (Table II and Fig. 1D), significant differences were found between arthritic and control L2 and L4 vertebras with regards to elastic (Young's) modulus, yield stress, ultimate stress and energy until yield stress, as compared to control vertebrae.

Bone collagen content is preserved during chronic arthritis

The SHG technique with MPM was not appropriate for the study of cortical bone as the images produced were homogenous and did not allow us to characterize the presence and organization of collagen molecules. However, images obtained in vertebral trabecular bone were very informative. Five control and 5 arthritic vertebrae were used to study bone collagen

Table I. Mean and standard deviation values calculated from mechanical tree-point bending test of mice female femurs.

	SKG mice (n=9)	BALB/c mice (n=8)	*p*-value
Diameter (mm)	1.10 ± 0.03	1.04 ± 0.02	0.001**
Stiffness (N/mm)	147.65 ± 18.87	197.84 ± 27.55	<0.001**
Yield stress (MPa)	108.68 ± 18.12	221.35 ± 62.72	0.001**
Ultimate stress (MPa)	171.57 ± 33.06	289.12 ± 48.28	<0.001**
Young's modulus (GPa)	6.79 ± 1.16	11.36 ± 1.96	0.001*
Ultimate strain (%)	5.69 ± 1.40	5.80 ± 1.50	0.564*
Energy until ultimate stress (N.mm/mm^3)	5.16 ± 2.32	8.30 ± 2.58	0.019**

Values are mean ± standard deviation.
*Mann-Whitney test.
**Independent-samples *t*-test.

content and structure. Quantitative image analysis of the collagen content showed no statistical differences between BALB/c control mice and SKG arthritic mice (Fig. 3A and 3B). The calculated percentage of collagen occupied areas depicted by forward-SHG channel in SKG and control vertebrae were 40.87±6.89% and 47.00±14.26%, respectively. This percentage was very similar to the one obtained by using the backward-SHG channel (52.81±6.05% and 53.90±11.03% for arthritic and control samples, respectively) (Fig. 3C). These percentages have to be calculated separately, as the channels in this imaging technique are individually analysed, so there is no direct correlation between values found for each group from the two channels. Furthermore, the ratio of mature collagen to immature collagen (the percentage obtained in the forward-SHG channel dividing by the one obtained in the backward -SHG channel) was of 0.775±0.179 for arthritic animals and 0.907±0.363 for control bones (*p*-value of 0.372).

As mature polymerised collagen has a signal present predominantly in the forward-SHG channel and amorphous collagen fibril segments in the backward-SHG channel one can assume that the relative distribution of these two types of collagen and the total amount of collagen per bone surface are equivalent in the arthritic and control groups. However, qualitative analysis of mice vertebrae using SHG microscopy revealed structural differences in the mature collagen organization in the arthritic group images in comparison to controls. In fact, in the SKG mice (arthritic group) areas of a nodular pattern in the collagen organization were observed among the longitudinal fibrils of the mature collagen (Fig. 3A and 3B).

Vertebrae from arthritic mice have a higher inter-trabecular distance and a decreased trabeculae thickness

In arthritic SKG mice vertebrae the trabeculae thickness was reduced giving rise to an increased inter-trabecular distance in comparison to BALB/c mice vertebrae, as highlighted by SEM images (Table III and Fig. 4). Moreover, vertebral cortical thickness was significantly lower in the SKG bone as compared to the controls. However, the trabeculae area, as assessed by SEM, was similar between the 2 groups.

Chronic arthritis reduces bone density

The density measurements were lower in the arthritic group as compared to the control group (Table IV). These results were statistically different for femurs and L2 vertebrae.

Mineral bone composition is not affected by arthritis

The results from the EDS analysis did not reveal any significant difference in the bone mineral composition in terms of calcium and phosphorous proportion between the arthritic and control bone samples, both in femurs (arthritic femur: calcium = 73% (72-75%) and phosphorus = 27% (25-28%); control femur: calcium = 73% (73-74%); and phosphorus = 27% (26-27%); no statistically significant differences between groups) and in vertebrae (arthritic vertebrae: calcium = 72% (42-79%) and phosphorus = 28% (21-58%); control vertebrae: calcium = 71% (52-79%);

Table II. Mean and standard deviation values calculated from mechanical compression stress-strain curves of female mice vertebrae L2 and L4.

	L2			L4		
	SKG mice (n=7)	BALB/c mice (n=6)	*p*-value	SKG mice (n=7)	BALB/c mice (n=5)	*p*-value
Height (mm)	2.82 ± 0.39	3.28 ± 0.46	0.077*	3.23 ± 0.25	3.67 ± 0.30	0.015*
Diameter (mm)	2.99 ± 0.15	2.97 ± 0.14	0.824*	2.82 ± 0.14	2.96 ± 0.07	0.063*
Young's Modulus (MPa)	20.17 ± 4.74	42.60 ± 18.70	0.007**	16.81 ± 2.33	30.29 ± 16.28	0.138*
Yield stress (MPa)	2.14 ± 0.61	3.85 ± 1.39	0.029*	2.06 ± 1.08	4.45 ± 1.83	0.028**
Energy until yield stress (Nmm/mm^3)	0.13 ± 0.08	0.22 ± 0.10	0.109*	0.12 ± 0.09	0.30 ± 1.15	0.028**
Maximum stress (MPa)	4.73 ± 0.92	6.89 ± 1.58	0.015**	3.35 ± 1.09	6.13 ± 0.87	0.005**
Energy until maximum stress (Nmm/mm^3)	1.13 ± 0.68	1.10 ± 0.54	0.668**	0.66 ± 0.15	0.57 ± 0.17	0.268**

Values are mean ± standard deviation.
*Mann-Whitney test; **Independent-samples *t*-test.

and phosphorus = 29% (24-48%); no statistically significant differences between groups).

Discussion

It is well established that RA is associated with secondary osteoporosis and an increased risk of fractures. This is apparently the end result of multiple factors, such as the use of corticosteroids, aging, menopause and inflammation. Thus, the direct contribution of the effect of chronic inflammation on bone in RA patients is difficult to assess. The primary aim of this study was to assess the influence of chronic inflammation in the SKG mouse chronic arthritis model on the biomechanical strength of the bone. The secondary aim was to study femoral bones and vertebral bodies, using new methods to assess the effect of chronic inflammation on the collagen and mineral structure of bone tissue. This is the first report in the literature demonstrating a deleterious and direct effect of chronic inflammation *per se* on the biomechanical quality of bone. This may in part clarify the increased fracture risk in RA patients.

Due to the anatomical qualities of the femoral bones and vertebral bodies it was necessary to use two different types of tests to measure their biomechanical strength. First, the femoral bones were tested using a three point bending test. In this test increasing force is applied to the femoral shaft using a cross-head. This leads first to fully elastic deformation of the bone so that if the force is released, the bone assumes its former shape. This property of the bone is usually expressed as its elastic Young's modulus and the maximum stress still enabling such reversible changes is referred to as the yield point. When more stress is applied, bone tissue starts to undergo microfractures and truly irreversible plastic changes occur, as it is characteristic of a ductile material. Upon release of the stress force, it can be observed that the morphological bone changes are now permanent. The maximum stress the bone can tolerate without breakage reveals its ultimate strength, after which a macroscopic fracture soon follows. In this study, it was for the first time shown that arthritic

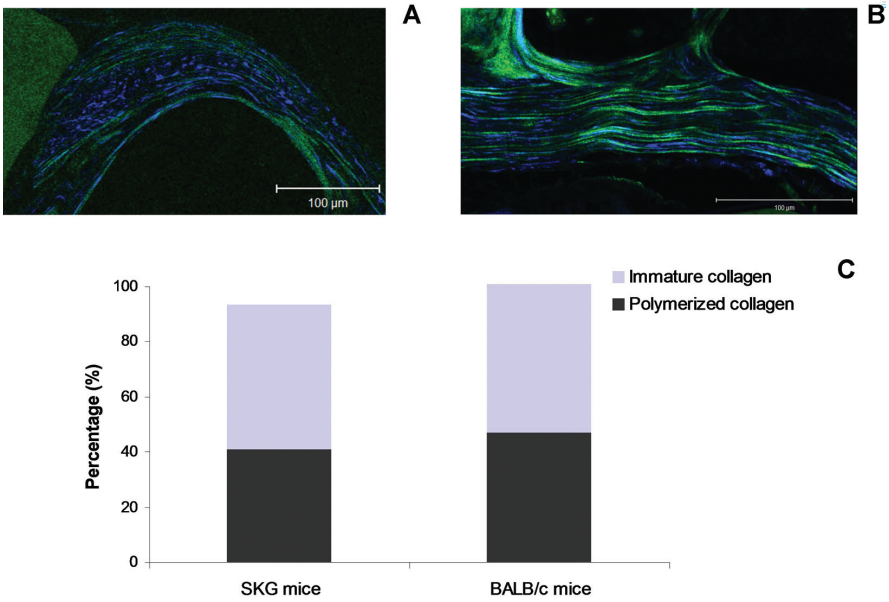

Fig. 3. Multiphoton microscopy images obtained from **(A)** SKG mouse vertebrae and **(B)** BALB/c mouse vertebrae. The green colour (backward-SHG channel) corresponds to immature collagen fibril segments, indicating ongoing fibrillogenesis and the blue colour (forward-SHG channel) corresponds to the mature polymerized collagen. **(C)** The content of collagen in the vertebrae was not affected by arthritis. Scale bars correspond to 100µm.

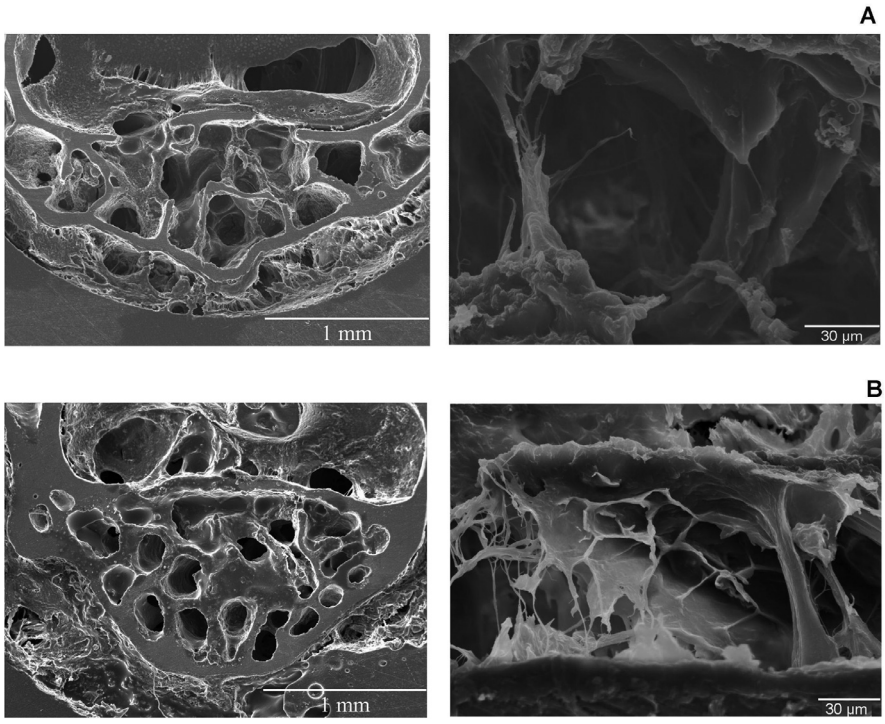

Fig. 4. Vertebrae from arthritic mice have a decreased trabeculae thickness and a higher inter-trabecular distance. Scanning electron microscopy images from female mice vertebrae with (A) and (B) without arthritis, showing a higher inter-trabecular distance and a decreased trabeculae thickness. Scale bars correspond to 1mm (left) and 30µm (right).

femoral bones have impaired elasticity, ductility and ultimate (fracture) strength compared to healthy control femoral bones. In accordance with these results, the compression test used to characterize the biomechanics of the vertebral bodies also showed impairment in the arthritic mice. This could be expected by the low trabeculae area of the cancellous vertebral bone (SEM analysis) as well as by the abnormal nodular structural organisation of its collagen

Table III. Trabeculae and cortical measurements of lumbar vertebrae, as determined by scanning electron microscopy.

	SKG mice (n=6)	BALB/c mice (n=4)	*p*-value
Cortical thickness (μm)	82.40 ± 23.71	99.81 ± 27.44	<0.001*
Trabeculae occupied area (%)	18.91 ± 5.39	21.63 ± 8.22	0.540**
Trabeculae thickness (μm)	57.18 ± 16.78	70.91 ± 23.66	<0.001*
Inter-trabecular distance (μm)	218.92 ± 88.18	188.04 ± 72.54	0.017*

Values are mean ± standard deviation.
*Mann-Whitney test; **Independent-samples t-test.

Table IV. Density measurements for femurs and vertebra.

	SKG mice (n=6)	BALB/c mice (n=7)	*p*-value
Femur density (g/cm^3)	1.17 ± 0.02	1.35 ± 0.07	0.002**
Vertebra L2 density (g/cm^3)	0.82 ± 0.10	0.94 ± 0.07	0.034*
Vertebra L4 density (g/cm^3)	0.89 ± 0.08	1.03 ± 0.25	0.268*

Values are mean ± standard deviation.
*Mann-Whitney test; **Independent-samples t-test.

architecture in the vertebral bone (SHG analysis). However, differences might be even greater than the ones depicted by our results as the squared vertebral body is supported by a slowly remodelling cortical bone shell, which, as a strong and stiff structure, protects the more vulnerable trabeculae bone interior and could mask the impact of the mechanical test.

Interestingly, SHG, independently both in the forward and backward mode, as well as the SEM-coupled EDS methods disclosed that the bulk collagen content and relative proportions of bone embedded minerals do not differ between arthritis and healthy controls. Although the reasons for the impaired quality of arthritic bone remain at present unclear, based on the current work it seems that they may relate to the mineral content and quality (architecture) of bone rather than to its total collagen content or the composition of the hydroxyapatite laid down in the organic bone matrix.

The results of this study clearly show that chronic inflammation directly induces a reduction in bone density and a change in the pattern of bone organization. This is the first report to indicate that arthritis is associated with an impairment of the bone mechanical properties, namely impaired elasticity, ductility and ultimate (fracture) strength. These observations encourage pharmacological intervention studies to analyze if it would be possible to counteract these arthritis-associated and fracture-predisposing changes by targeting also the bone metabolism, apart from controlling the arthritis itself.

References

1. ALAMANOS Y, DROSOS AA: Epidemiology of adult rheumatoid arthritis. *Autoimmun Rev* 2005; 4: b130-6.
2. NEUMANN E, GAY S, MULLER-LADNER U: The RANK/RANKL/osteoprotegerin system in rheumatoid arthritis: new insights from animal models. *Arthritis Rheum* 2005; 52: 2960-7.
3. ORSTAVIK RE, HAUGEBERG G, MOWINCKEL P *et al*.: Vertebral deformities in rheumatoid arthritis: a comparison with population-based controls. *Arch Intern Med* 2004; 164: 420-5.
4. VAN STAA TP, GEUSENS P, BIJLSMA JW *et al*.: Clinical assessment of the long-term risk of fracture in patients with rheumatoid arthritis. *Arthritis Rheum* 2006; 54: 3104-12.
5. RAISZ LG: Pathogenesis of osteoporosis: concepts, conflicts, and prospects. *J Clin Invest* 2005; 115: 3318-25.
6. LAMGHARI M, TAVARES L, CAMBOA N *et al*.: Leptin effect on RANKL and OPG expression in MC3T3-E1 osteoblasts. *J Cell Biochem* 2006; 98: 1123-9.
7. HORWOOD NJ, KARTSOGIANNIS V, QUINN JM *et al*.: Activated T lymphocytes support osteoclast formation in vitro. *Biochem Biophys Res Commun* 1999; 265: 144-50.
8. FONSECA JE, CORTEZ-DIAS N, FRANCISCO A *et al*.: Inflammatory cell infiltrate and RANKL/OPG expression in rheumatoid synovium: comparison with other inflammatory arthropathies and correlation with outcome. *Clin Exp Rheumatol* 2005; 23: 185-92.
9. THEILL LE, BOYLE WJ, PENNINGER JM: RANK-L and RANK: T cells, bone loss, and mammalian evolution. *Annu Rev Immunol* 2002; 20: 795-823.
10. VIGUET-CARRIN S, GARNERO P, DELMAS PD: The role of collagen in bone strength. *Osteoporos Int* 2006; 17: 319-36.
11. PEREL P, ROBERTS I, SENA E *et al*.: Comparison of treatment effects between animal experiments and clinical trials: systematic review. *BMJ* 2007; 334: 197.
12. HIROTA K, HASHIMOTO M, YOSHITOMI H *et al*.: T cell self-reactivity forms a cytokine milieu for spontaneous development of IL-17+ Th cells that cause autoimmune arthritis. *J Exp Med* 2007; 204: 41-7.
13. SAKAGUCHI N, TAKAHASHI T, HATA H *et al*.: Altered thymic T-cell selection due to a mutation of the ZAP-70 gene causes autoimmune arthritis in mice. *Nature* 2003; 426: 454-60.
14. AKHTER MP, CULLEN DM, GONG G *et al*.: Bone biomechanical properties in prostaglandin EP1 and EP2 knockout mice. *Bone* 2001; 29: 121-5.
15. HELMCHEN F, DENK W: Deep tissue two-photon microscopy. *Nat Methods* 2005; 2: 932-40.
16. JEFFERIES Z, KLINE AH, ZIMMER EB: The determination of grain size in metals. *Trans AIME* 1916; 57: 594-607.
17. WILLIAMS RM, ZIPFEL WR, WEBB WW: Interpreting second-harmonic generation images of collagen I fibrils. *Biophys J* 2005; 88: 1377-86.